Published in final edited form as:
Eur J Neurosci. 2010 August ; 32(3): 383–398. doi:10.1111/j.1460-9568.2010.07279.x.

Broca's Region: Linking Human Brain Functional Connectivity Data and Nonhuman Primate Tracing Anatomy Studies

Clare Kelly[1,*], **Lucina Q. Uddin**[2,*], **Zarrar Shehzad**[1], **Daniel S. Margulies**[3], **F. Xavier Castellanos**[1,4], **Michael P. Milham**[1,4], and **Michael Petrides**[5]

[1] The Phyllis Green and Randolph Cowen Institute for Pediatric Neuroscience, New York University Child Study Center, New York, NY 10016

[2] Department of Psychiatry, Stanford University School of Medicine, Stanford, CA 94304

[3] Berlin School of Mind and Brain, Humboldt Universitat, Berlin, Germany

[4] The Nathan Kline Institute for Psychiatric Research, 140 Old Orangeburg Road, Orangeburg, NY 10962, United States

[5] Montreal Neurological Institute, McGill University, Montreal, Quebec, Canada, H3A2B4

Abstract

Brodmann areas 6, 44, and 45 in the ventrolateral frontal cortex of the left hemisphere of the human brain constitute the anterior language production zone. The anatomic connectivity of these areas with parietal and temporal cortical regions was recently examined in an autoradiographic tract-tracing study in the macaque monkey. Studies suggest strong correspondence between human resting state functional connectivity (RSFC) based on functional magnetic resonance imaging data and experimentally demonstrated anatomical connections in non-human primates. Accordingly, we hypothesized that areas 6, 44 and 45 of the human brain would exhibit patterns of RSFC consistent with patterns of anatomical connectivity observed in the macaque. In a primary analysis, we examined the RSFC associated with regions-of-interest placed in ventrolateral frontal areas 6, 44 and 45, on the basis of local sulcal and gyral anatomy. We validated the results of the primary hypothesis-driven analysis with a data-driven partitioning of ventrolateral frontal cortex into regions exhibiting distinct RSFC patterns, using a spectral clustering algorithm. The RSFC of ventrolateral frontal areas 6, 44 and 45 was consistent with patterns of anatomical connectivity shown in the macaque. We observed a striking dissociation between RSFC for the ventral part of area 6 that is involved in orofacial motor control and RSFC associated with Broca's region (areas 44 and 45). These findings indicate rich and differential RSFC patterns for the ventrolateral frontal areas controlling language production, consistent with known anatomical connectivity in the macaque brain, and suggest conservation of connectivity during the evolution of the primate brain.

Keywords

fMRI; resting state; inferior frontal gyrus; language; clustering

Correspondence should be addressed to: Michael P. Milham, 215 Lexington Avenue, 14th Floor, New York, NY 10016, michael.milham@nyumc.org. Michael Petrides, 3801 University Street, Montreal, Quebec, H3A2B4, Canada, michael.petrides@mcgill.ca.
*These two authors contributed equally to the manuscript.

Introduction

The ventrolateral frontal region, which includes Brodmann areas 6, 44 and 45, in the left hemisphere of the human brain, has been implicated in language processing since Broca's (1861) description of the eponymous speech disorder. Later, Wernicke (1874) suggested that posterior temporal cortex is important for the receptive aspects of language, leading to the concept of a fronto-temporal language circuit linked via the arcuate fasciculus (Geschwind, 1970). Research on the effects of lesions and electrical stimulation during brain surgery, and recent functional neuroimaging studies, have shown that the posterior language zone includes not only posterior temporal cortex, but also the supramarginal and angular gyri of the inferior parietal lobule (Penfield & Roberts, 1959; Rasmussen & Milner, 1975; Ojemann *et al.*, 1989; Binder *et al.*, 1997). Explorations of the structural connectivity of these regions with diffusion tensor imaging (DTI; Catani *et al.*, 2005; Croxson *et al.*, 2005; Frey *et al.*, 2008; Saur *et al.*, 2008) suggest that, in addition to the classical arcuate fasciculus, ventrolateral frontal cortex interacts with inferior parietal lobule via the superior longitudinal fasciculus and the lateral temporal cortex via the extreme capsule fasciculus, as originally shown in the macaque monkey (Petrides & Pandya, 1984; 1988).

Although DTI studies can provide evidence about major white matter pathways, current methodological limitations do not allow precise delineation of the origins and terminations of these pathways. As such, experimental tracer studies in non-human primates remain the gold standard for uncovering the precise origins and terminations of cortico-cortical connections. Recently, resting state functional connectivity (RSFC) analyses, which detect coherent low-frequency fluctuations in the BOLD signal, have emerged as a valuable non-invasive method for mapping the functional circuitry of the brain that is complementary to DTI. Correspondence between RSFC and anatomical connectivity is not 1:1, as RSFC has been observed between regions lacking direct anatomical connections (Vincent *et al.*, 2007; Di Martino *et al.*, 2008; Uddin *et al.*, 2008). Nonetheless, patterns of functional and structural connectivity (measured with diffusion imaging) are convergent (reviewed by Damoiseaux & Greicius, 2009). Moreover, two recent studies have demonstrated remarkable consistency between patterns of RSFC in the human brain and maps of anatomical connectivity derived from experimental tracer studies in the macaque monkey (Vincent *et al.*, 2007; Margulies *et al.*, 2009).

Here, we examine the hypothesis that the patterns of RSFC between areas 6, 44 and 45 and posterior parietal and temporal regions in the human brain are comparable with patterns of anatomical connectivity between the homologues of these areas in the macaque monkey, established in a recent autoradiographic study (Petrides & Pandya, 2009). In order to test this overarching hypothesis, we performed a seed-based RSFC analysis in which the placement of seed regions-of-interest was determined on an individual basis according to sulcal and gyral morphology. We thus aimed to adopt a level of rigor similar to that exemplified by autoradiographic anatomical studies, albeit limited by the spatial resolution permitted by fMRI. We followed this primary examination with a data-driven spectral clustering analysis to verify distinctions emerging from the seed-based analysis.

Materials and Methods

Participants

Thirty-six healthy right-handed adult subjects, aged 20–52 (19 females, 17 males, mean age = 28.1 ± 7.9), participated in this study. All subjects were free of psychiatric disorders or history of head trauma. Participants signed informed consent after the experimental procedures were explained and received monetary compensation. The study complied with the Code of Ethics of the World Medical Association (Declaration of Helsinki) and was

approved by the Institutional Review Boards at New York University and the NYU School of Medicine. Data from these participants have been included in previously published studies (e.g., Margulies *et al.*, 2007; Di Martino *et al.*, 2008; Shehzad *et al.*, 2009).

fMRI Data Acquisition

Images were acquired on a Siemens Allegra 3-Tesla scanner using an EPI gradient echo sequence (TR = 2000ms; TE = 25ms; Flip angle = 90, 39 slices, matrix 64×64; FOV = 192mm; acquisition voxel size 3×3×3mm, 197 volumes, duration = 6min 38s) while subjects rested with eyes open. A T1-weighted anatomical image was also acquired for registration purposes (MP-RAGE, TR = 2500ms; TE = 4.35ms; TI = 900ms; Flip angle = 8; 176 slices; FOV = 256mm, acquisition voxel size 1×1×1mm).

fMRI Data Analysis

Image preprocessing—Slice timing correction (for interleaved acquisition), motion correction, despiking, temporal band pass filtering (0.009–0.1Hz), and quadratic detrending using linear least squares, were performed using AFNI (Cox, 1996). Further image preprocessing steps were completed using FSL (www.fmrib.ox.ac.uk), and comprised spatial smoothing (using a Gaussian kernel of FWHM 6 mm) and mean-based intensity normalization of all volumes by the same factor (each subject's entire four-dimensional (4-D) dataset was scaled by its global mean).

Registration of high resolution structural images to the MNI152 template (Montreal Neurological Institute) with $2mm^3$ resolution was carried out using the FSL linear registration tool FLIRT (Jenkinson & Smith, 2001; Jenkinson *et al.*, 2002). Transformation to MNI152 standard space was then further refined using FNIRT nonlinear registration (Andersson *et al.*, 2007a; b). Linear registration of each participant's functional time series to the space of the high-resolution structural image was also carried out using FLIRT.

Nuisance signal regression—To control for the effects of physiological processes (such as fluctuations related to cardiac and respiratory cycles) and motion, we removed signal associated with several nuisance covariates. Specifically, we regressed each subject's preprocessed 4-D volume on nine predictors that modeled nuisance signals from white matter (WM), cerebrospinal fluid (CSF), the global signal, and six motion parameters, as detailed elsewhere (Kelly *et al.*, 2009).

This nuisance signal regression step produced a 4-D residuals volume for each participant. As a final preprocessing step, each participant's 4-D residuals volume was spatially normalized by applying the previously computed transformation to MNI152 standard space, with 1 mm^3 resolution.

Method 1 For RSFC Analysis: Hypothesis-Driven Seed-Based RSFC

Summary of Ventrolateral Frontal ROI Selection: In order to best delineate the patterns of RSFC associated with ventral area 6 and areas 44 and 45, the precise placement of the three ventrolateral frontal ROIs was determined on an individual basis. Specifically, to maximize the probability that the ROIs would lie in architectonic areas 44, 45, and ventral area 6, we followed a two-step procedure. First, we examined each participant's normalized (to MNI152 space) high-resolution structural MRI image and used sulcal landmarks to identify the pars opercularis (BA 44), pars triangularis (BA 45), and the ventral part of the anterior precentral region for premotor BA 6 (described in detail below). Although the depth of the sulci may not always coincide with architectonic boundaries (Fischl *et al.*, 2008; Lohmann *et al.*, 2008), all studies that have examined the cytoarchitecture of the inferior frontal gyrus agree that the bulk of the pars opercularis is occupied by area 44, while the bulk of the pars

triangularis is occupied by area 45 (e.g., Brodmann, 1909; Petrides & Pandya, 1994; Amunts *et al*., 1999; Petrides & Pandya, 2002).

Subsequent to the initial identification step, we adjusted our placement of the ROIs according to details of the local morphology of each particular brain. This second adjustment step was necessary in order to ensure that the ROIs would not be placed close to the sulci where there is ambiguity about the exact border between areas, but rather in a part of the pars opercularis, pars triangularis and rostral inferior precentral gyrus where all available architectonic studies agree that areas 44 and 45 and ventral area 6 are located. For instance, Amunts et al. (1999) have shown that the border of area 44 and ventral area 6 can vary within the inferior precentral sulcus. Thus, we made sure that the ROIs for areas 44 and 6 were clearly away from the inferior precentral sulcus in each individual brain and were located within the pars opercularis and the inferior precentral gyrus at positions where all architectonic studies (including those of our own laboratory; Petrides & Pandya, 1994; 2002) agree that areas 44 and 6 are located.

The specific criteria used for placement of the three ventrolateral frontal ROIs are described in detail below. For each participant, once the desired placement of the three ventrolateral frontal ROIs was identified, a spherical ROI with a 2mm radius was created using the AFNI program 3dUndump.

Brodmann's Area 44: Most of BA 44 lies on the pars opercularis of the inferior frontal gyrus (e.g., Brodmann, 1909; Petrides & Pandya, 1994; Amunts *et al.*, 1999; Petrides & Pandya, 2002), which is defined caudally by the inferior precentral sulcus, rostrally by the ascending ramus of the Sylvian fissure and dorsally by the inferior frontal sulcus. Furthermore, according to the probabilistic map of BA44 by Amunts et al. (1999), and the probabilistic map of the pars opercularis by Tomaiuolo et al. (1999), BA 44 lies between y = 12 and y =14 in the left hemisphere, in MNI standard stereotaxic space. Our first step in ROI placement was therefore to identify BA 44, using these sulcal landmarks and coordinates as guidelines. The second step was to examine the local morphology of the particular brain and to make adjustments to the ROI placement as necessary. For instance, because the precise location of the border between area 44 and ventral area 6 can vary, we made sure that we placed the area 44 ROI clearly in front of the inferior precentral sulcus. In addition, we know that the pars opercularis is often divided into an anterior and posterior part by the diagonal sulcus (Keller *et al.*, 2007) and Amunts et al. (1999) have reported that in some brains area 44 stops at the diagonal sulcus. Thus, if in a particular brain the diagonal sulcus was present, we placed the ROI posterior to this sulcus to avoid possible overlap with the anteriorly adjacent BA 45. Finally, we aimed to place the center of the ROI in the middle of the pars opercularis in the dorsal-ventral direction, between z = 10 and z = 20, thus avoiding unintended overlap with cortex lying above the inferior frontal sulcus.

Brodmann's Area 45: Unlike the pars opercularis, which is a clearly delimited part of the inferior frontal gyrus, the morphology of the pars triangularis, where BA 45 lies, is more variable. The pars triangularis lies rostral to the ascending sulcus and dorsal to the horizontal sulcus. Dorsally, it is delimited partly by the rostral part of the inferior frontal sulcus. Our first step in ROI placement was therefore to identify BA 45 using these sulcal landmarks, between y = 24 and y= 26, just above the horizontal sulcus, at around z = 0. The exact position of the ROI was then adjusted according to the local sulcal morphology of the particular brain and knowledge of the relation of these sulci and architectonic area 45 obtained from our human architectonic studies (Petrides & Pandya, 1994; 2002) and other published studies (Amunts *et al.*, 1999) to maximize the probability that our ROI would be sampling BA 45 cortex.

Brodmann's Area 6: For the ventral part of BA 6, we placed the center of the ROI in the rostral part of the ventral precentral gyrus, clearly caudal to the inferior precentral sulcus (around y = 6), at approximately the same dorsal-ventral level as the ROI for BA 44 for that particular brain, i.e. between z = 10 and z = 20. We know that in the ventral half of the inferior precentral gyrus, the primary motor cortex (area 4) lies mostly within the anterior bank of the central sulcus and most of the crown of the ventral precentral gyrus is occupied by BA 6. Thus, by placing the seed in the anterior part of the ventral precentral gyrus (but away from the inferior precentral sulcus to avoid overlap with BA 44), we were maximizing the probability that the ROI would be sampling BA 6.

Resting State Functional Connectivity (RSFC): For each participant, a mean BOLD time series was extracted for each of the three ventrolateral frontal ROIs (BA 6, BA 44, BA 45) by averaging across all voxels within the ROI. We then used the AFNI program 3dfim+ to compute the correlation between each time series and every other voxel in the brain. Group-level maps of positive RSFC for each ROI were computed using a one-sample t-test (against 0), and corrected for multiple comparisons using the FSL program easythresh ($Z > 2.3$; cluster significance $p < 0.05$, corrected). Direct comparisons between the maps were computed using paired t-tests, and were also corrected for multiple comparisons using the FSL program easythresh ($Z > 2.3$; cluster significance $p < 0.05$, corrected).

Method 2 For RSFC Analysis: Data-Driven Spectral Clustering: In a second approach, we used data-driven clustering methods in order to verify distinctions between ventrolateral frontal areas 6, 44, and 45 on the basis of their RSFC (i.e., the results of the primary, hypothesis-driven seed-based analysis). Clustering algorithms are used to partition (classify) data into natural subsets (clusters) such that observations assigned to the same cluster are more similar to one another than they are to observations assigned to another cluster. In the context of RSFC, clustering algorithms have been used to partition the brain into subsets (clusters) of voxels or regions that are functionally connected with one another (e.g., van den Heuvel *et al*., 2008a), or that exhibit similar patterns of functional connectivity with the rest of the brain (Cohen et al., 2008). Here, we adopted the latter approach, and used spectral and hierarchical clustering algorithms to assign voxels within a ventrolateral frontal ROI (419 voxels in total) to clusters on the basis of a measure of the similarity between their whole-brain correlation maps (eta^2).

The starting point for the clustering analysis was to establish the left ventrolateral frontal ROI which comprised the inferior precentral gyrus (inferior to z = 30), the pars opercularis, the pars triangularis, and the remaining inferior frontal gyrus (as defined by the Harvard-Oxford atlas) posterior to y = 50. The ROI comprised 419 voxels, each one being 4×4×4mm in size.

Measure of similarity: eta^2: We computed the whole-brain RSFC associated with each one of the 419 voxels within the ventrolateral ROI, using the same methods described above. We then computed the similarity between every possible pairing of the 419 RSFC maps, using eta^2. The eta^2 statistic was recently applied to RSFC data for this purpose by Cohen et al. (2008), and varies between 0 (no similarity) and 1 (identical). Cohen et al. suggested that eta^2 provides a better measure of similarity between two images than spatial correlation, because it can take into account differences in scaling and offset between two images, while correlation is unaffected by these factors. We computed a 419×419 eta^2 matrix describing the similarity between each pair of the 419 RSFC maps for every participant (36 in total).

Clustering Analyses: We used the spectral clustering toolbox written for Matlab by Verma and Meila (available at http://www.stat.washington.edu/spectral/) to partition the left ventrolateral frontal ROI into *K* clusters, where *K* ranged from 2 to 10. Specifically, we used

the Meila-Shi (multicut) algorithm (Meila & Shi, 2001), which performs a generalized Eigen decomposition of the normalized Lagrangian of similarity matrix *A* (here, the 419×419 eta^2 matrix), then applies the k-means clustering algorithm to partition the data on the basis of *K* highest eigenvectors. The eigenvectors of the similarity matrix provide information about the data's structure. By performing partitional clustering (with k-means) on the basis of these eigenvectors, spectral clustering makes use of this information (the data's *spectrum*) in order to form clusters of voxels that maximize intra-cluster similarity (here, eta^2) and minimize inter-cluster similarity. For comparison, we also partitioned the data using standard hierarchical clustering, as implemented in the Matlab Statistics toolbox. Hierarchical clustering is an agglomerative method, which starts by treating each data point as a singleton cluster, then, as *K* decreases, successively merges previously established clusters (visualized as a dendrogram or tree). Here, we formed clusters of voxels on the basis of average linkage, that is, the unweighted average of the distances (1-eta^2) between all pairs of voxels, where one member of the pair is assigned to one cluster and the other member is assigned to a different cluster. At each iteration, *K* clusters are formed by merging the two clusters (from the *K*+1 solution) exhibiting the smallest average distances.

Clustering the Group-Average eta^2 Matrix: In order to determine the optimal *K* for the ventrolateral ROI, we used a split-half comparison procedure. First, we randomly assigned each of the 36 participants to one of two groups of 18 participants. Then, *for each group*, we: (1) calculated the group-average of the 18 single-subject eta^2 matrices, and (2) applied the spectral and hierarchical clustering algorithms to identify cluster solutions for the range *K* = 2:12. For each value of *K*, we compared the cluster solutions generated for Group 1 and Group 2 using a metric developed for assessing the similarity of cluster assignments: Variation of Information (VI; Meila, 2007). We repeated the entire process 100 times, each time generating two new groups of 18 participants. We determined the optimal *K* (or range of *K*) by computing the mean VI across the 100 permuted groups, for each *K*, and selecting the non-trivial (i.e., $K > 2$) solution that showed the lowest mean VI. The mean VI across solutions also allowed us to determine which of the two algorithms (spectral or hierarchical) produced the most consistent solution. The results of the above-described analysis suggested that the spectral clustering algorithm produced more consistent clustering solutions (associated with the lowest mean VI) across the permuted groups, relative to the hierarchical clustering algorithm (**see Results**). Accordingly, we used the spectral clustering algorithm for the remaining analyses.

Modified Silhouette: To further discern the optimal *K*, we calculated a modified silhouette value for each value of *K*, for cluster solutions produced when the spectral clustering algorithm was applied *to each individual's* eta^2 matrix. The silhouette is a standard metric, which provides, for each point (in our case, voxel), a measure of how similar it is to other points within the same cluster, versus how similar it is to points in other clusters. In the following equation, eta_{wi} corresponds to the mean of the eta^2 values describing the similarity between **voxel *i*** and **voxels** in other clusters.

$$S(i)=\frac{(\min(1-eta_{bi}))-(1-eta_{wi})}{\max((1-eta_{wi}),\min(1-eta_{bi}))}$$

Instead of estimating a voxel-wise *S*, we estimated a modified *cluster-wise* silhouette value in order to provide a summary measure of the similarity of points within a **cluster**, relative to the similarity between **clusters**:

$$\tilde{S}\ (k)=\frac{(\min(1-eta_{bk}))-(1-eta_{wk})}{\max((1-eta_{wk}),\min(1-eta_{bk}))}$$

In the equation for $\tilde{S}$, eta_{wk} corresponds to the *mean* eta^2 value describing the similarity between all voxels within cluster *k* ($eta_{i\in k,\ j\in k}$):

$$eta_{wk}=\frac{\sum eta_{i\in k,\ j\in k}}{n_k * n_k}$$

while eta_{bk} corresponds to the *K*-1 *mean* eta^2 values describing the similarity between all pairings of voxels within cluster *k* ($eta_{i\in k}$) and voxels within other clusters ($eta_{j\notin k}$):

$$eta_{bk_i}=\frac{\sum eta_{i\in k_i,\ j\notin k_i}}{n_{k_i} * n_{\notin k_i}}$$

To compute the mean Modified Silhouette, we first applied the spectral clustering algorithm to each participant's eta^2 matrix, to identify cluster solutions for the range *K* = 2:12. We then performed the calculations described above, to compute the Modified Silhouette for each value of K and for each participant. We then plotted the mean and standard deviation, across participants.

Effect of Smoothing: During data preprocessing, we applied a 6mm FWHM Gaussian spatial smoothing filter. To assess whether smoothing affects cluster assignment, we repeated the analyses and eta^2 matrix generation without spatial smoothing. We applied the spectral clustering algorithm to the *group-average* of all (*n* = 36) single-subject unsmoothed eta^2 matrices, and assessed the similarity between the solutions reached on the basis of the smoothed and unsmoothed data using the VI metric.

Consensus Matrix Clustering: An alternative approach to cluster validation is to perform clustering on an individual subject level and to examine the stability with which pairs of voxels are assigned to the same cluster, across individuals (e.g., Steinley, 2008).

We applied the spectral clustering algorithm to each individual subject's eta^2 matrix, to identify cluster solutions for the range *K* = 2: 12 at the single-subject level. For each subject (*s*), and each *K*, we constructed an adjacency matrix,

$$A^{(s)}=\left(a_{ij}^{(s)}\right)_{419\times 419}$$

where $a_{ij}^{(s)}=1$ if voxels *i* and *j* are assigned to the same cluster *k*, and 0 otherwise. For each *K*, we then computed a consensus matrix,

$$A^{(\bar{S})}=\frac{1}{S}\sum_{s=1}^{S}A^{(s)}$$

such that each element of the 419×419 consensus matrix corresponds to the proportion of times a given pair of voxels appeared in the same cluster, across participants.

To discern the most stable pattern of cluster assignment across subjects, we applied the spectral clustering algorithm to the 12 resultant consensus matrices. For each *K*'s consensus matrix we identified the cluster solution, using the same *K*, and compared the quality of the cluster assignments using the modified silhouette metric (where the silhouette was calculated on the basis of the mean within- vs. between-cluster consensus values, rather than the eta^2 values). Finally, we assessed the similarity between the solutions reached on the basis of the consensus matrices to those reached on the basis of the group-average of the single-subject eta^2 matrices, using the VI metric.

Seeding the K = 4 spectral clustering solution: The clustering validation methods suggested that the most favorable clustering solution was that produced by the spectral clustering algorithm for $K = 4$ (see Results). To verify the distinctions among the regions of ventrolateral frontal cortex suggested by this clustering solution, we created four spherical seed ROIs of diameter 8mm, centered on the centers-of-mass of each of the clusters of the group-average $K = 4$ spectral clustering solution. We computed the group-level RSFC for each of the seeds, and performed direct comparisons between seeds in the same manner as for the manually selected ventrolateral prefrontal seeds ($Z > 2.3$; cluster significance $p < 0.05$, corrected).

Results

Seed ROI Results

Brodmann's Area 44—The ROI placed in BA 44 exhibited robust positive correlations with the pars triangularis (BA 45) and pars orbitalis (area 47/12) of the inferior frontal gyrus (IFG), as well as with the inferior premotor region (BA 6). In addition, there were positive correlations with the pre-supplementary motor area (preSMA), the paracingulate region (BA 32) and the adjacent medial frontal cortex (BAs 8, 9) (Fig. 1). There were also correlations with the caudal dorsolateral frontal cortex (BA 8) and the rostral part of dorsal BA 6. In the parietal cortex, correlations were primarily restricted to the ventral part of the posterior supramarginal gyrus (pSMG) and the adjacent angular gyrus. In the temporal lobe, there were significant correlations with the caudal part of the superior temporal gyrus (STG), the superior temporal sulcus (STS), and with the middle temporal gyrus (MTG). There were no correlations with primary somatomotor cortex within the central sulcus or the somatomotor cortical region around the medial extension of the central sulcus, i.e., paracentral lobule BA 4. There were also no significant correlations with the superior parietal lobule, the posterior cingulate, precuneus, and ventromedial prefrontal regions.

Brodmann's Area 45—The ROI in BA 45 exhibited a pattern of positive correlations similar to that of BA 44 (Fig. 1). BA 45 exhibited significant correlations with BAs 44 and 47/12 in the inferior frontal gyrus, as well as with the posterior dorsolateral frontal region (BA 8) and dorsal BA 6. In the parietal cortex, there were positive correlations with the ventral part of the posterior supramarginal gyrus (pSMG) and the angular gyrus. In the temporal lobe, there were strong positive correlations with the caudal superior temporal gyrus, the entire superior temporal sulcus and middle temporal gyrus. Medially, BA 45 exhibited positive correlations with the pre-supplementary motor area, the paracingulate region (BA 32) and the medial frontal region (BAs 8, 9, and 10). In addition, there were robust correlations with the ventromedial frontal region. There were no correlations with primary somatomotor cortex within the central sulcus or the somatomotor cortical region around the medial extension of the central sulcus, i.e., paracentral lobule BA 4. There were

also no significant correlations with the superior parietal lobule, the posterior cingulate region, or precuneus.

Ventral Precentral Gyrus (BA 6)—The ventral BA 6 ROI, located in the ventral part of the precentral gyrus, close to the inferior precentral sulcus, was positively correlated with BAs 44 and dorsal 45, as well as a region of the middle frontal gyrus (MFG) that lies just above the pars triangularis, and which was termed area 9/46v by Petrides and Pandya (1994). Significant positive correlations were also observed between BA 6 and the adjacent motor and somatosensory cortex within the central sulcus, as well as the medial extension of the somatomotor region on the paracentral lobule. There were also positive correlations with the secondary somatosensory region in the frontal and parietal opercula and the insula. Correlations extended to the superior temporal gyrus (STG) and the posterior-most part of the middle temporal gyrus (MTG). Within the posterior parietal cortex, positive correlations were primarily restricted to the anterior part of the supramarginal gyrus (aSMG). On the medial surface of the brain, the seed in BA 6 was correlated with the supplementary motor region (medial BA 6) as well as the ventrally adjacent cortex within the cingulate sulcus and gyrus that correspond to the cingulate motor areas discovered in the macaque monkey (He *et al.*, 1995). Notably, the BA 6 seed did not exhibit any correlations with the medial frontal cortex (i.e., BAs 8, 9, 10) or the ventromedial prefrontal cortex. There were also no positive correlations with the posterior cingulate cortex or precuneus (Fig. 1).

Direct contrasts: BA 45 > BA 44 and BA 44 > BA 45—To examine the differences between BA 44 and BA 45, direct contrasts were carried out between these two ROIs. Relative to BA 44, BA 45 exhibited greater positive correlations with the pars orbitalis region of the inferior frontal gyrus where area 47/12 is located (see Petrides and Pandya, 1994), with the ventromedial prefrontal cortex, and with the angular gyrus. Note that on the surface of the brain, this stronger RSFC appears to be restricted to the dorsal part of the angular gyrus, but this is simply the result of the fact that much of the correlated activity lies just below the cortex and within the parietal extension of the superior temporal sulcus which will not show on the surface of the brain, as can be seen in the appropriate coronal section in Fig. 2 (BA 45 > BA 44). BA 44 exhibited greater RSFC (relative to BA 45) with the premotor BA 6, the secondary somatosensory cortex within the upper bank of the Sylvian fissure, and the caudal superior temporal gyrus (Fig. 1, Table 1).

The above RSFC results were in excellent agreement with the predictions of connectivity from parietal and temporal cortex to the homologous ventrolateral regions in the macaque monkey based on the experimental anatomical study of these connections (Petrides and Pandya, 2009). However, there was also an apparent contradiction. In the study with the macaque monkey, the connections of area 45 with lateral temporal cortex appeared to be more widespread than those of area 44 and to include a more ventral component of the lateral temporal cortex. Comparison of the surface of the brain in Fig. 2 (compare panels BA 45 and BA 44) appears to confirm this greater activity in the lateral temporal cortex for BA 45 than BA 44. However, this did not reach the accepted level of significance in the direct comparison BA 45 > BA 44. Given our prediction that differential RSFC would be observed, we repeated the direct comparison between BA 44 and 45 RSFC, restricting our analysis to the left temporal lobe ($Z > 2.3$; cluster significance $p < 0.05$, corrected for a volume of 22768mm^3). This restricted comparison did reveal significantly greater RSFC between BA 45 and the middle temporal gyrus, relative to BA 44 (Fig. 2).

Direct contrasts: BA 6 > BA 44 and BA 6 > BA 45—To examine the differences between BA 6 and BAs 44 and 45, direct contrasts were carried out between these ROIs. Relative to both BAs 44 and 45, BA 6 exhibited stronger RSFC with primary somatic and motor areas around the central sulcus, and the secondary somatosensory areas within the

frontal and parietal opercula, and the insula. There were also stronger correlations between BA 6 and the superior parietal lobule and the anterior part of the supramarginal gyrus (aSMG), relative to both BAs 44 and 45. There were stronger correlations between BA 6 and the supplementary motor region (SMA) and the motor region in the central cingulate gyrus and sulcus which probably correspond to the cingulate motor areas discovered in the macaque monkey (He *et al.*, 1995) (Fig. 1, Table 1).

Direct contrasts: BA 44 > BA 6 and BA 45 > BA 6—Relative to BA 6, BAs 44 and 45 exhibited stronger correlations with the pars orbitalis of the inferior frontal gyrus (area 47/12) and the caudal dorsolateral frontal cortex corresponding to BA 8 (Fig. 1, Table 1). In the temporal lobe, there were significantly stronger correlations with the cortex within the superior temporal sulcus and the middle temporal gyrus. On the medial surface, BAs 44 and 45 showed stronger correlations than BA 6 with medial frontal cortex anterior to the SMA involving BAs 8, 9, and 10, as well as the paracingulate BA 32. Additionally, BA 45 exhibited stronger RSFC with the medial part of the frontal pole (BA 10), the ventromedial frontal cortex, and the angular gyrus, relative to BA 6, while BA 44 did not show these differences.

Clustering Results

Clustering the Group-Average eta^2 Matrix—Using a permuted-groups split-half comparison procedure, we applied spectral and hierarchical clustering algorithms to identify cluster solutions for the range $K = 2{:}12$, where K is the number of clusters. For each value of K, we assessed the similarity of the cluster solutions generated for Group 1 ($n = 18$) and Group 2 ($n = 18$) using the Variation of Information (VI) metric (Meila, 2007). Fig 3D plots the mean VI across 100 permuted groups, for each K, and each clustering algorithm. The results indicate that the most similar (consistent) solutions (associated with the lowest mean VI) were generated by the spectral clustering algorithm. The most consistent non-trivial solution (i.e., $K>2$) appears to be $K=4$, though there is good mean similarity for the range $K = 2{:}6$.

We subsequently applied the spectral clustering algorithm to the group-average of all ($n = 36$) single-subject eta^2 matrices. Fig. 4 displays the surface maps for the spectral clustering solutions for $K = 2{:}6$ (for comparison, the surface maps of the hierarchical clustering solutions for $K = 2{:}6$ are presented in Supplementary Fig. S1).

Modified Silhouette—To further discern the optimal K, we calculated a modified silhouette value for each value of K, for cluster solutions produced when the spectral clustering algorithm was applied *to each individual's* eta^2 matrix. As shown in Fig. 3E, the Modified Silhouette criterion suggested that $K=4$ represents the most favorable solution.

Effect of Smoothing—To assess the impact of smoothing on cluster assignment, we repeated the analyses and eta^2 matrix generation without spatial smoothing. Fig. 4 shows the surface maps for the spectral clustering solutions for $K = 2{:}6$, computed on the basis of group-average of unsmoothed eta^2 matrices (Fig. 3B). Qualitatively, the maps are highly similar, a conclusion which is supported quantitatively by the VI metric (Fig. 3H), which indicates good similarity between the smoothed and unsmoothed solutions for K 7.

Consensus Matrix Clustering—In a second approach to cluster validation, we performed spectral clustering on an individual subject level, then examined the stability with which pairs of voxels were assigned to the same cluster across individuals, by computing a consensus matrix (Steinley, 2008), an example of which is shown in Fig. 3C. To discern the most stable pattern of cluster assignment across subjects, we applied the spectral clustering

algorithm to the consensus matrices and computed the Modified Silhouette. Fig. 3F plots the Modified Silhouette values, and suggests that, across subjects, the most stable pattern of cluster assignment is for $K = 4$. Qualitatively, the surface maps for the solutions computed on the basis of the consensus matrix are highly similar to those computed on the basis of the group-average eta^2 matrix (Fig. 4), and the VI metric demonstrates the best similarity between the clustering solutions is for $K = 2{:}4$ (Fig. 3G).

Seeding the *K* = 4 cluster solution—On the basis of the clustering analyses, we concluded that $K = 4$ represented the most favorable solution (see Fig. 4). Qualitatively, the four clusters were located in the superior part of the inferior frontal gyrus (IFG), bordering the inferior frontal sulcus (Cluster 1); the lateral pars opercularis and pars triangularis (Cluster 2); inferior precentral cortex (Cluster 3); and a fourth region extending medially within the Sylvian fissure from the inferior-most tip of ventral premotor cortex and the pars opercularis towards the anterior insula (Cluster 4). To verify these clusters as functionally distinct regions of ventrolateral frontal cortex, we examined the RSFC associated with four spherical seed ROIs of 4mm radius, centered on the centers-of-mass of each of the clusters of the group-average $K = 4$ spectral clustering solution. Fig. 5 shows the group-level ($Z > 2.3$; cluster significance $p < 0.05$, corrected)RSFC for each of the four clusters, as well as direct comparisons between clusters.

The pattern of RSFC observed for Cluster 2 that includes the central parts of the pars opercularis and pars triangularis is very similar to those observed for ROIs based in BAs 44 and 45 (compare Cluster 2 in Fig. 5 with BA 44 and 45 in Fig. 1). Similarly, the pattern of RSFC for Cluster 3 that includes the inferior part of the precentral gyrus is consistent with that for the ROI based in BA 6 (compare Cluster 3 in Fig. 5 with BA 6 in Fig. 1). The voxels in Cluster 1 probably separate from the rest of the large ventrolateral frontal region of interest that was defined for the clustering analysis by virtue of the fact they are located along the inferior frontal sulcus on the border with the middle frontal gyrus which would include voxels of areas 8 and 9/46v in the upper bank of the inferior frontal sulcus and adjacent middle frontal gyrus. Specifically, Cluster 1 exhibited RSFC with almost all of the inferior frontal gyrus, anterior to and including the inferior precentral sulcus, dorsal BA 6 and BA 8 in the middle frontal gyrus, the intraparietal sulcus, and the caudal middle and inferior temporal cortex. The comparison Cluster 1 > Cluster 2 (Fig. 5) isolates this border region in the frontal lobe and highlights the stronger RSFC with the intraparietal sulcus for voxels that may belong to area 8 and 9/46 in comparison with voxels that are more likely to lie in areas 45 and 44. Finally, Cluster 4 exhibited a pattern of RSFC similar to that of Cluster 2, but with less extensive RSFC with the lateral temporal lobe and the medial frontal cortex, and more extensive RSFC with the dorsal cingulate gyrus and supplementary motor areas, as well as anterior frontal cortex. It may represent a region that would include voxels in the anterior insula region and the frontal opercular region.

Overall, the patterns of RSFC associated with the $K = 4$ spectral clustering solution were consistent with those of the primary seed-based analysis of the ventrolateral frontal regions, and confirmed a significant distinction between premotor BA 6 and BAs 44 and 45, but greater similarity than difference between BAs 44 and 45 in terms of their RSFC.

Discussion

The traditional view of the cortical language circuit has been of a ventrolateral frontal speech zone (Broca's area) in the left hemisphere of the human brain that is linked with a language comprehension zone in the posterior superior temporal region via the arcuate fasciculus (Geschwind, 1970). However, several lines of evidence suggest that cortical language circuits must be much more complex than the classical scheme. Electrical

stimulation studies during brain surgery and functional neuroimaging studies have shown that the posterior language zone is very wide and includes not only posterior superior temporal cortex, but also the superior temporal sulcus and the adjacent middle temporal gyrus, as well as the supramarginal and angular gyri of the inferior parietal lobule (e.g., Penfield & Roberts, 1959; Rasmussen & Milner, 1975; Ojemann *et al.*, 1989; Binder *et al.*, 1997). Furthermore, the ventrolateral frontal language production zone includes three distinct parts: the ventral part of the premotor zone (BA 6) that is involved with the control of the orofacial musculature, as well as area 44 and area 45 that together comprise Broca's region. Electrical stimulation of ventral premotor area 6 results in vocalization, while stimulation of area 44 and the caudal part of area 45 results in speech arrest (e.g., Penfield & Roberts, 1959; Rasmussen & Milner, 1975; Ojemann *et al.*, 1989). Establishing the similarities and differences in connectivity of these three ventrolateral frontal areas involved in language production with the perisylvian posterior parietal and temporal regions that constitute the posterior language zone, is critical to our understanding of the neural networks underlying language processing.

Experimental anatomical tracing studies in the macaque monkey have shown that a major branch of the superior longitudinal fasciculus links the inferior parietal region with the ventrolateral frontal region (Petrides & Pandya, 1984) and a major pathway running in the extreme capsule links the lateral temporal region with the ventrolateral frontal region (Petrides & Pandya, 1988). Recent DTI studies have also succeeded in demonstrating these pathways in the human brain (e.g., Catani *et al.*, 2005; Croxson *et al.*, 2005; Makris *et al.*, 2005; Anwander *et al.*, 2007; Frey *et al.*, 2008; Makris & Pandya, 2009) and evidence is beginning to emerge that they are involved in language related processing (e.g., Saur *et al.*, 2008). However, DTI analyses do not currently permit delineation of the precise origins and terminations of pathways from *specific cortical areas* and thus limit the extent to which the similarities and differences in connectivity of areas 6, 44 and 45 can be revealed using that method alone. Resting state functional connectivity (RSFC) analyses offer complementary information concerning patterns of inter-regional connectivity, and there is increasing evidence to suggest that patterns of RSFC track (to a large extent, although not in a 1:1 manner) underlying anatomical connectivity (Vincent *et al.*, 2007; Skudlarski *et al.*, 2008; van den Heuvel *et al.*, 2008b; Honey *et al.*, 2009; Margulies *et al.*, 2009; van den Heuvel *et al.*, 2009). Here, we used RSFC to test hypotheses about the connectivity of the ventrolateral frontal areas with parietal and temporal cortex in the human brain derived from experimental anatomical studies of the macaque monkey.

Predictions from experimental studies of cortico-cortical connections in the monkey

The recent demonstration of the homologues of Broca's area in the macaque monkey ventrolateral frontal cortex (Petrides *et al.*, 2005) has permitted the utilization of experimental anatomical tracing to explore the details of the connectivity of these areas with the posterior perisylvian parietal and temporal regions using the autoradiographic method (Petrides & Pandya, 2009). Tract tracing studies in the macaque have shown that ventral premotor region BA 6 (which is critical for orofacial motor control) is strongly connected with the most anterior part of the inferior parietal lobule, which exhibits a distinct architecture and is known as area PF in the monkey. By contrast, areas 44 and 45 are strongly connected with more posterior inferior parietal lobule areas which, in the monkey, are referred to as areas PFG and PG (Petrides, 2006; Petrides & Pandya, 2009). Based on comparative architectonic studies, area PF of the macaque monkey corresponds to the anterior part of the supramarginal gyrus in the human, whereas area PFG corresponds to the human posterior supramarginal gyrus and area PG to the human angular gyrus (Petrides and Pandya, unpublished observations).

The macaque studies have also shown that areas 44 and 45 are strongly linked with the cortex in the superior temporal sulcus and the ventrally adjacent temporal cortex, which in the human brain corresponds to the middle temporal gyrus. Petrides and Pandya (2009) showed that, in the macaque, although areas 44 and 45 have similar anatomical connectivity with posterior parietal and temporal areas, there are differences in emphasis. Specifically, in the macaque, area 45 has stronger connections than area 44 with area PG (corresponding to the human angular gyrus) and stronger connections than area 44 with the temporal cortex that lies within and below the superior temporal sulcus (which corresponds to the middle temporal gyrus of the human brain).

These findings in the macaque monkey provide strong predictions of differential functional connectivity in the human brain that are testable using RSFC data. We hypothesized that the patterns of functional connectivity between areas 6, 44 and 45 and posterior temporal and parietal regions in the human brain would exhibit a degree of specificity similar to that established for connections between the homologues of these areas in the macaque monkey, using the autoradiographic method. To test this hypothesis, we performed an *a-priori* seed-based functional connectivity analysis of human resting state data, in which the precise placement of seed regions of interest in areas 6, 44 and 45 was determined on an individual basis according to sulcal and gyral morphology. We then verified the observed distinctions between the patterns of RSFC exhibited by these regions by performing a data-driven spectral clustering analysis, in which we partitioned the inferior frontal region-of-interest into groups of voxels exhibiting similar patterns of RSFC.

The results of these two analyses were consistent with one another, and with the predictions from the experimental anatomical tracing studies in the macaque monkey. These findings indicate that the perisylvian parietal and temporal functional connectivity with left ventrolateral frontal cortex in the human brain maintains the same basic patterns observed in non-human primates. These patterns of connectivity are *schematically* summarized in Fig. 6.

Robust separation of ventral area 6 from areas 44 and 45

The present RSFC analyses demonstrated a striking dissociation between the pattern of RSFC associated with the ventral part of area 6 that is involved in orofacial control and the patterns of RSFC associated with the two areas that comprise Broca's region (areas 44 and 45). The RSFC profile of BA 6 was that of a motor zone – it exhibited functional connectivity with dorsal premotor cortex, the primary motor and somatosensory cortex within and around the central sulcus, the secondary somatosensory areas in the upper bank of the Sylvian fissure and, on the medial surface of the brain, the supplementary motor area and the cingulate motor areas. This pattern of RSFC (which is consistent with the known anatomical connectivity of ventral premotor area 6 established in monkey anatomical tracing studies) was not shared with areas 44 and 45.

Of particular interest was the RSFC of ventral area 6 with the supramarginal gyrus. In the macaque monkey, ventral area 6 exhibits strong cortico-cortical connections only with the most anterior part of the inferior parietal lobule (referred to as area PF) (Petrides & Pandya, 1984; Matelli *et al.*, 1986; Cavada & Goldman-Rakic, 1989; Cavada & Goldman-Rakic, 2009), while areas 44 and 45 of the monkey brain are linked more strongly with area PFG and PG that lie more caudally in the inferior parietal region (Petrides and Pandya, 2009) and correspond to the caudal supramarginal and angular gyri. This pattern of anatomical connectivity was confirmed with RSFC in the human brain and clearly set ventral area 6 apart from areas 44 and 45. As can be seen in Fig. 1, the functional connectivity of area 6 was restricted to the anterior part of the supramarginal gyrus that is delimited by the posterior ascending ramus of the Sylvian fissure. The pattern of RSFC associated with

Cluster 3 (Fig. 5) supports this conclusion, which was also confirmed by the direct contrasts between BA 6, BAs 44 and 45 (as shown in Fig. 1 and Table 1).

The strong RSFC of BA 6 with the most anterior part of the inferior parietal lobule and the absence of correlations with the posterior part of the supramarginal gyrus and the angular gyrus define a unique profile of parietal RSFC for ventral BA 6. By contrast, areas 44 and 45 exhibited a functional connectivity pattern with the posterior supramarginal gyrus and the angular gyrus (Fig. 1), consistent with predictions from the macaque monkey studies (Petrides & Pandya, 2009). Furthermore, areas 44 and 45 had strong correlations with the cortex in the superior temporal sulcus and the temporal cortex just below it, namely the middle temporal gyrus (Fig. 1, Fig. 2). The strong distinction between the connectivity patterns associated with ventral area 6, relative to areas 44 and 45 is most evident in the results of the clustering analysis. The simplest and most robust partitioning of the data (K=2, see Fig. 3), was one that separated ventral area 6 into one cluster, and areas 44, 45 and the rest of the inferior frontal gyrus into another (see top row of Fig. 4). The clear separation between ventral area 6 and area 44 anteriorly was also present for the optimal solution (K=4, see Fig. 4).

In both monkey and human brains, ventral area 6 is a typical premotor cortex that lacks layer IV, whereas area 45 is a typical prefrontal cortex with a well developed layer IV (Brodmann, 1909; Amunts *et al.*, 1999; Petrides & Pandya, 2002). Area 44, which lies between areas 6 and 45, does possess a layer IV, but it is interrupted and not well developed. Consequently, there has long been confusion as to whether BA 44 should be considered a premotor zone that is functionally similar to premotor cortex or whether BA 44 is functionally more similar to prefrontal BA 45. For instance, some investigators have considered Broca's region to include both BAs 44 and 45 (Amunts *et al.*, 1999) while others have restricted it to BA 44 (Mohr *et al.*, 1978). The present results address this issue. The functional connectivity patterns of BAs 44 and 45, which together comprise Broca's area, were more similar to one another than to the RSFC of ventral BA 6. This conclusion is also consistent with a recent study by Amunts and Zilles (2006), who examined the architectonic and neurochemical profiles of BA 44 and concluded that it shares more features with BA 45 than with BA 6. Furthermore, anatomical connectivity studies of the homologues of areas 44 and 45 in the macaque also show that these two areas have similar connection patterns and clearly differ in connectivity from ventral area 6 (Petrides & Pandya, 2009).

Functional connectivity of areas 44 and 45

Although areas 44 and 45 share a similar pattern of cortico-cortical connectivity that sets them apart from the caudally adjacent premotor area 6, they have some subtle but important differences in connectivity. The recent experimental anatomical tracer study (Petrides and Pandya, 2009) examining perisylvian parietal and temporal connections with the ventrolateral frontal region noted that connections from area PG (especially its dorsal part close to the intraparietal sulcus) were stronger with area 45. The same anatomical tracing study also noted that, although both areas 44 and 45 receive inputs from the cortex in the superior temporal sulcus, they differ in that area 45 (but not area 44) had strong connections with the ventrally adjacent temporal cortex. Although the RSFC of areas 44 and 45 were very similar (see Fig. 2, BA 44 and BA 45, and the results of the clustering analyses, Fig. 4), the direct comparison between areas 44 and 45 demonstrated greater RSFC of BA 45 in the dorsal part of the angular gyrus close to the intraparietal sulcus (see Fig. 2, BA 45 > BA 44, 3D brain surface and coronal section). However, these whole-brain comparisons did not reveal significantly greater RSFC in any part of the temporal lobe for BA 45 relative to BA 44. Given our *a priori* hypotheses concerning such a difference, we restricted our comparison to the superolateral temporal cortex (i.e. the cortex on the superior temporal gyrus, the superior temporal sulcus and the middle temporal gyrus), which is the zone

known to connect to the ventrolateral frontal region. This directed analysis did indeed demonstrate stronger RSFC between BA 45 and the middle portion of the middle temporal gyrus, relative to BA 44 (Fig. 2).

The present results provide a more complete picture of language-related cortico-cortical connections than the traditional view of a posterior superior temporal language zone that interacts with an anterior frontal speech zone via the arcuate fasciculus (Geschwind, 1970). Consistent with results from macaque tracer studies, the present findings show that only the inferior part of the parietal lobe interacts with the anterior language zone. Specifically, we demonstrated linkage between rostral supramarginal gyrus and ventral BA 6, and between the caudal supramarginal and angular gyri and BAs 44 and 45 in the human brain. Furthermore, we demonstrated greater linkage of the middle section of the middle temporal gyrus with BA 45 than BA 44, consistent with experimental findings in the macaque monkey (Petrides & Pandya, 1988).

Relevance for theories for language processing and production

The richer view of the cortico-cortical pathways linking language-related regions demonstrated here agrees with recent diffusion tensor imaging studies of the complexity of the white matter connectivity between these regions (Saur *et al.*, 2008; Makris & Pandya, 2009). It is also in agreement with theoretical views that suggest a dual stream model for auditory language processing (e.g., Hickok & Poeppel, 2004; Warren *et al.*, 2005). According to the dual stream model, initial auditory processing in the superior temporal gyrus proceeds via a dorsal stream to the inferior parietal lobule and then to the ventrolateral frontal region for auditory-motor integration, which is necessary for mapping the acoustic speech sounds to articulatory acts. At the same time, a ventral stream is hypothesized to map sounds to meaning in lateral temporal areas. A recent study (Saur *et al.*, 2008) combined fMRI during two prototypical tasks tapping dorsal (speech repetition) and ventral (language comprehension) streams with diffusion tensor imaging. The authors showed that fibers of the arcuate fasciculus and the superior longitudinal fasciculus are indeed linked to speech repetition and those of the extreme capsule to language comprehension. A clearer understanding of how different zones of language-related cortex are linked together, using both DTI and RSFC approaches, will have a major impact on our understanding of the neural circuits underlying various aspects of linguistic processing.

The primary purpose of the present study was to examine the correspondence between the RSFC of the anterior language production zone, comprising left ventrolateral frontal areas 6, 44 and 45, and the findings of a recent autoradiographic tract tracing study that established the anatomical connections between the homologues of these areas and perisylvian parietal and temporal cortex in the macaque (Petrides & Pandya, 2009). As such, we limited our primary analyses to the ventrolateral frontal areas 6, 44 and 45. However, area 47/12 (Petrides, 2005), located on the pars orbitalis, also plays a role in human language processing, particularly in higher level aspects of semantic processing that rely on memory retrieval (Petrides & Pandya, 2002). Although beyond the scope of this study, the RSFC related to area 47/12 and its consonance with or differentiation from the RSFC exhibited by surrounding cortical areas, such as area 45, is an issue that should be explored in future studies.

The human mirror neuron system

“Mirror neurons” were initially described by Rizzolatti and colleagues in monkey ventral premotor cortex (Gallese *et al.*, 1996; Rizzolatti *et al.*, 1996) and later in inferior parietal cortex (Fogassi *et al.*, 2005). The defining characteristic of these neurons is that they discharge during the execution of certain actions, but also during the observation of a similar

action performed by another agent (Rizzolatti & Craighero, 2004). For example, if a mirror neuron discharges when the monkey grasps an object, it will also fire when the monkey observes another agent (human experimenter) grasping the same object.

Mirror neurons were originally observed in area F5 of the monkey (Gallese *et al.*, 1996; Rizzolatti *et al*., 1996), which is the homologue of ventral area 6, extending into area 44 in the human, as well as in area PF in the rostral part of the inferior parietal lobule (Fogassi *et al.*, 2005), corresponding to human anterior supramarginal gyrus. We have shown that, in the human, ventral area 6 exhibits a specific pattern of RSFC with anterior supramarginal gyrus that is distinct from the pattern of RSFC exhibited by area 44 (and area 45). This network may thus constitute the human analogue of the mirror neuron system. Area 44, which is linked to ventral area 6, may provide (in the language dominant hemisphere) the means by which semantic information retrieved from memory controls action intended to convey a linguistic message (Petrides, 2002; 2006).

Previous studies of ventrolateral-perisylvian RSFC

Previous studies have demonstrated significant RSFC between ventrolateral and perisylvian areas (e.g., Dosenbach *et al.*, 2007; Fair *et al.*, 2007; Vincent *et al.*, 2008), and two previous studies specifically examined the functional connectivity of Broca's area (Hampson *et al.*, 2002; Xiang *et al.*, 2009). Xiang et al. used a seed ROI-based RSFC analysis in a small sample of 12 participants to demonstrate topographical functional organization in Broca's area. The authors reported substantial overlap in functional connectivity patterns of pars opercularis and pars triangularis, consistent with the results of our study. Similarly, Hampson et al. demonstrated significant functional connectivity between Broca's area, defined as all voxels within BAs 44 and 45 activated when listening to continuous speech, and Wernicke's area, defined as those activated voxels in the superior temporal gyrus and angular gyrus. However, neither of these previous studies aimed to examine differential functional connectivity of the ventrolateral frontal areas, and therefore did not show the striking dissociation that we observed between ventral area 6 and the two areas that are traditional considered to constitute Broca's region, namely areas 44 and 45. Furthermore, the present study was able to confirm the subtle differences in RSFC between areas 44 and 45, based on predictions of patterns of anatomical connectivity obtained from experimental tracer studies in the macaque (Petrides & Pandya, 2009), that were not noted in those previous studies.

Clustering approaches to RSFC

Here, we demonstrated the potential utility of voxel-wise RSFC-based clustering as an objective, data-driven approach for characterizing functional differentiation in structurally and functionally complex brain regions, such as ventrolateral frontal cortex. The partitions emerging from our examination of the ventrolateral frontal region (Fig. 4), as well as the subsequent ROI-based RSFC analysis (Fig. 5), provided additional support for the distinctions between areas 6, 44 and 45 that were demonstrated using the *a priori* ROIs (Fig. 1). Importantly, we demonstrated that the clustering solutions were not dependent on spatial smoothing.

A similar confirmatory clustering analysis was previously performed by Margulies et al. (2009) in their comparison of posteromedial cortex RSFC in the human and the macaque monkey. Our approach represents an advance on that of Margulies et al., however. Specifically, while Margulies et al. partitioned posteromedial cortex by clustering their *a priori* seed regions, we performed clustering of the ventrolateral region on a voxel-wise basis. We thereby allowed distinctions between ventrolateral subregions to emerge directly from the data, without the imposition of any *a priori* restrictions on the partitioning, beyond

the selection of the ventrolateral region-of-interest itself. There is considerable potential for the application of this approach to other functionally heterogeneous regions of the brain, such as anterior cingulate cortex, in order to elucidate their complex functional architecture in an objective, data-driven manner.

Along with others (van den Heuvel *et al.*, 2008a; Bellec *et al.*, 2010), the present work demonstrates the utility of performing cluster analyses at the individual participant level, computing a consensus matrix representing the consistency of cluster assignment across the group, then deriving the group-level clustering solutions on the basis of that consensus matrix. Focusing on the consensus matrix in this way may be particularly important for areas characterized by relatively high morphometric interindividual variability, such as ventrolateral frontal cortex (Amunts *et al.*, 1999; Tomaiuolo *et al.*, 1999; Keller *et al.*, 2007).

Despite their utility, clustering analyses are subject to the same core limitation as other model-free approaches – namely, parameter estimation. Because of the lack of *a priori* knowledge concerning the "true" number of clusters (i.e., the true *K*), a range of cluster solutions must be tested and reported. This is very similar to the requirement to examine varying threshold levels in network analyses, and varying levels of dimensionality in independent components analysis. Future work focusing on methods for optimizing estimates for the clustering parameters would be beneficial.

Limitations

The anatomical basis of RSFC extends beyond direct, monosynaptic neuronal connectivity, to include polysynaptic connections (Vincent *et al.*, 2007; O'Reilly *et al.*, 2009). It has been previously observed that functional connections can exist where no direct structural connections are present (Uddin *et al.*, 2008; Vincent *et al.*, 2008; Honey *et al.*, 2009; Roy *et al.*, 2009). Although the patterns of RSFC observed in the present study were consistent with predictions from monosynaptic pathways in the macaque monkey, we observed some correlations that were not consistent with known anatomical connectivity in the monkey. Such "additional" connectivity may, at least in part, be due to the spatial resolution of our data (acquisition voxel size was 3×3×3mm, which is typical of whole-brain functional MRI studies), and the application of spatial smoothing (also standard, FWHM = 6mm). On the other hand, the physiological bases of RSFC remain incompletely understood, and a more complete understanding may shed light on the bases of these patterns of RSFC.

Likewise, it is likely that our analyses may have missed even more subtle differences in functional connectivity that may exist between BAs 44 and 45, due to factors such as spatial smoothing, or the limits of our image resolution. However, the data-driven clustering analyses also did not distinguish between BAs 44 and 45 on the basis of their RSFC, even when the analyses were repeated using data that had not been spatially smoothed. Thus, it does not appear that the failure to distinguish between these two areas is due to the smoothness of the data. Future studies may consider acquiring data with greater spatial resolution than the 3×3×3mm voxel size employed in the present study. Another possibility is that the considerable interindividual variability in morphometry of the ventrolateral frontal region (i.e., the presence or absence of particular sulci and gyri, and their arrangement; Amunts *et al.*, 1999; Tomaiuolo *et al.*, 1999; Keller *et al.*, 2007) may have contributed to these findings. However, we took several steps to minimize the impact of such variability, including manual determination of seed placement on the basis of local sulcal and gyral anatomy, and use of non-linear registration to the template (MNI) brain. Finally, as methods for integrating information about both structural (e.g., DTI) and functional connectivity are developed, we may be better able to elucidate the subtle distinctions between adjacent, functionally similar regions such as BAs 44 and 45.

Concluding Remarks

To summarize, we observed a striking dissociation between the orofacial component of the ventral premotor cortex (BA 6) and Broca's region (BAs 44 and 45) in terms of their patterns of RSFC that was consistent with predictions from experimental anatomical studies of the monosynaptic connectivity of homologous areas in the macaque monkey. We were also able to uncover some of the differences in functional connectivity between areas 44 and 45. These observations add to a growing list of studies, anatomical and functional, that are changing the traditional conceptualization of how the different components of Broca's region interact with parietal and temporal cortical areas that are involved in different aspects of language processing. These results also provide further support for the utility of resting state functional connectivity in delineating complex neural circuits in the human brain *in vivo*.

Supplementary Material

Refer to Web version on PubMed Central for supplementary material.

Acknowledgments

We would like to thank Pierre Bellec, Alexander Cohen, and Cameron Craddock for helpful discussions and suggestions.

Funding Statement

This study was partially supported by grants from the Stavros Niarchos Foundation, National Institute of Mental Health (R21MH066393, T32MH067763) to F.X.C. and by the Leon Levy Foundation (F.X.C. and M.P.M.), a CIHR grant (MOP-14620) to M.P. and a National Institute on Drug Abuse grant (R03DA024775-01) awarded to C.K. L.Q.U. is supported by a Mosbacher Postdoctoral Fellowship and NIMH award number K01MH092288.

References

Amunts K, Schleicher A, Burgel U, Mohlberg H, Uylings HB, Zilles K. Broca's region revisited: cytoarchitecture and intersubject variability. J Comp Neurol. 1999; 412:319–341. [PubMed: 10441759]

Amunts, K.; Zilles, K. A multimodal analysis of structure and function in Broca's region. In: Grodzinsky, Y.; Amunts, K., editors. Broca's Region. Oxford University Press; New York: 2006.

Andersson JLR, Jenkinson M, Smith SM. Non-linear optimisation. FMRIB technical report TR07JA1. 2007a

Andersson JLR, Jenkinson M, Smith SM. Non-linear registration, aka Spatial normalisation. FMRIB technical report TR07JA2. 2007b

Anwander A, Tittgemeyer M, von Cramon DY, Friederici AD, Knosche TR. Connectivity-Based Parcellation of Broca's Area. Cereb Cortex. 2007; 17:816–825. [PubMed: 16707738]

Bellec P, Rosa-Neto P, Lyttelton OC, Evans AC. Multi-level bootstrap analysis of stable clusters in resting-state fMRI. Neuroimage. 2010 Epub ahead of print. 10.1016/j.neuroimage.2010.02.082

Binder JR, Frost JA, Hammeke TA, Cox RW, Rao SM, Prieto T. Human brain language areas identified by functional magnetic resonance imaging. J Neurosci. 1997; 17:353–362. [PubMed: 8987760]

Broca P. Remarques sure le siége de la faculté du langage articulé; suivies d'une observation d'aphemie. Bull Soc Anat Paris. 1861; 6:330–357.

Brodmann, K. Vergleichende Lokalisationslehre der Grosshirnrinde in ihren Prinzipien dargestellt auf Grund des Zellenbaues. Barth; Leipzig: 1909.

Catani M, Jones DK, ffytche DH. Perisylvian language networks of the human brain. Ann Neurol. 2005; 57:8–16. [PubMed: 15597383]

Cavada C, Goldman-Rakic PS. Posterior parietal cortex in rhesus monkey: II. Evidence for segregated corticocortical networks linking sensory and limbic areas with the frontal lobe. J Comp Neurol. 1989; 287:422–445. [PubMed: 2477406]

Cohen AL, Fair DA, Dosenbach NU, Miezin FM, Dierker D, Van Essen DC, Schlaggar BL, Petersen SE. Defining functional areas in individual human brains using resting functional connectivity MRI. Neuroimage. 2008; 41:45–57. [PubMed: 18367410]

Cox RW. AFNI: software for analysis and visualization of functional magnetic resonance neuroimages. Comput Biomed Res. 1996; 29:162–173. [PubMed: 8812068]

Croxson PL, Johansen-Berg H, Behrens TE, Robson MD, Pinsk MA, Gross CG, Richter W, Richter MC, Kastner S, Rushworth MF. Quantitative investigation of connections of the prefrontal cortex in the human and macaque using probabilistic diffusion tractography. J Neurosci. 2005; 25:8854–8866. [PubMed: 16192375]

Damoiseaux JS, Greicius MD. Greater than the sum of its parts: a review of studies combining structural connectivity and resting-state functional connectivity. Brain Struct Funct. 2009; 213:525–533. [PubMed: 19565262]

Di Martino A, Scheres A, Margulies DS, Kelly AM, Uddin LQ, Shehzad Z, Biswal B, Walters JR, Castellanos FX, Milham MP. Functional connectivity of human striatum: a resting state FMRI study. Cereb Cortex. 2008; 18:2735–2747. [PubMed: 18400794]

Dosenbach NU, Fair DA, Miezin FM, Cohen AL, Wenger KK, Dosenbach RA, Fox MD, Snyder AZ, Vincent JL, Raichle ME, Schlaggar BL, Petersen SE. Distinct brain networks for adaptive and stable task control in humans. Proc Natl Acad Sci U S A. 2007; 104:11073–11078. [PubMed: 17576922]

Fair DA, Schlaggar BL, Cohen AL, Miezin FM, Dosenbach NU, Wenger KK, Fox MD, Snyder AZ, Raichle ME, Petersen SE. A method for using blocked and event-related fMRI data to study "resting state" functional connectivity. Neuroimage. 2007; 35:396–405. [PubMed: 17239622]

Fischl B, Rajendran N, Busa E, Augustinack J, Hinds O, Yeo BT, Mohlberg H, Amunts K, Zilles K. Cortical folding patterns and predicting cytoarchitecture. Cereb Cortex. 2008; 18:1973–1980. [PubMed: 18079129]

Fogassi L, Ferrari PF, Gesierich B, Rozzi S, Chersi F, Rizzolatti G. Parietal lobe: from action organization to intention understanding. Science. 2005; 308:662–667. [PubMed: 15860620]

Frey S, Campbell JS, Pike GB, Petrides M. Dissociating the human language pathways with high angular resolution diffusion fiber tractography. J Neurosci. 2008; 28:11435–11444. [PubMed: 18987180]

Gallese V, Fadiga L, Fogassi L, Rizzolatti G. Action recognition in the premotor cortex. Brain. 1996; 119 (Pt 2):593–609. [PubMed: 8800951]

Geschwind N. The organization of language and the brain. Science. 1970; 170:940–944. [PubMed: 5475022]

Hampson M, Peterson BS, Skudlarski P, Gatenby JC, Gore JC. Detection of functional connectivity using temporal correlations in MR images. Hum Brain Mapp. 2002; 15:247–262. [PubMed: 11835612]

He SQ, Dum RP, Strick PL. Topographic organization of corticospinal projections from the frontal lobe: motor areas on the medial surface of the hemisphere. J Neurosci. 1995; 15:3284–3306. [PubMed: 7538558]

Hickok G, Poeppel D. Dorsal and ventral streams: a framework for understanding aspects of the functional anatomy of language. Cognition. 2004; 92:67–99. [PubMed: 15037127]

Honey CJ, Sporns O, Cammoun L, Gigandet X, Thiran JP, Meuli R, Hagmann P. Predicting human resting-state functional connectivity from structural connectivity. Proc Natl Acad Sci U S A. 2009; 106:2035–2040. [PubMed: 19188601]

Jenkinson M, Bannister P, Brady M, Smith S. Improved optimization for the robust and accurate linear registration and motion correction of brain images. Neuroimage. 2002; 17:825–841. [PubMed: 12377157]

Jenkinson M, Smith S. A global optimisation method for robust affine registration of brain images. Med Image Anal. 2001; 5:143–156. [PubMed: 11516708]

Keller SS, Highley JR, Garcia-Finana M, Sluming V, Rezaie R, Roberts N. Sulcal variability, stereological measurement and asymmetry of Broca's area on MR images. J Anat. 2007; 211:534–555. [PubMed: 17727624]

Kelly C, de Zubicaray G, Di Martino A, Copland DA, Reiss PT, Klein DF, Castellanos FX, Milham MP, McMahon K. L-dopa modulates functional connectivity in striatal cognitive and motor networks: a double-blind placebo-controlled study. J Neurosci. 2009; 29:7364–7378. [PubMed: 19494158]

Lohmann G, von Cramon DY, Colchester AC. Deep sulcal landmarks provide an organizing framework for human cortical folding. Cereb Cortex. 2008; 18:1415–1420. [PubMed: 17921455]

Makris N, Kennedy DN, McInerney S, Sorensen AG, Wang R, Caviness VS Jr, Pandya DN. Segmentation of subcomponents within the superior longitudinal fascicle in humans: a quantitative, in vivo, DT-MRI study. Cereb Cortex. 2005; 15:854–869. [PubMed: 15590909]

Makris N, Pandya DN. The extreme capsule in humans and rethinking of the language circuitry. Brain Struct Funct. 2009; 213:343–358. [PubMed: 19104833]

Margulies DS, Kelly AM, Uddin LQ, Biswal BB, Castellanos FX, Milham MP. Mapping the functional connectivity of anterior cingulate cortex. Neuroimage. 2007; 37:579–588. [PubMed: 17604651]

Margulies DS, Vincent JL, Kelly C, Lohmann G, Uddin LQ, Biswal BB, Villringer A, Castellanos FX, Milham MP, Petrides M. Precuneus shares intrinsic functional architecture in humans and monkeys. Proc Natl Acad Sci U S A. 2009

Matelli M, Camarda R, Glickstein M, Rizzolatti G. Afferent and efferent projections of the inferior area 6 in the macaque monkey. J Comp Neurol. 1986; 251:281–298. [PubMed: 3021823]

Meila M. Comparing clusterings: an information-based distance. J Multivariate Analysis. 2007; 98:873–895.

Meila, M.; Shi, J. A random walks view of spectral segmentation. 8th International Workshop on Artificial Intelligence and Statistics (AISTATS); City.

Mohr JP, Pessin MS, Finkelstein S, Funkenstein HH, Duncan GW, Davis KR. Broca aphasia: pathologic and clinical. Neurology. 1978; 28:311–324. [PubMed: 565019]

O'Reilly JX, Beckmann CF, Tomassini V, Ramnani N, Johansen-Berg H. Distinct and Overlapping Functional Zones in the Cerebellum Defined by Resting State Functional Connectivity. Cereb Cortex. 2009

Ojemann G, Ojemann J, Lettich E, Berger M. Cortical language localization in left, dominant hemisphere. An electrical stimulation mapping investigation in 117 patients. J Neurosurg. 1989; 71:316–326. [PubMed: 2769383]

Penfield, W.; Roberts, L. Speech and Brain Mechanisms. Princeton University Press; Princeton, NJ: 1959.

Petrides M. The mid-ventrolateral prefrontal cortex and active mnemonic retrieval. Neurobiol Learn Mem. 2002; 78:528–538. [PubMed: 12559832]

Petrides M. Lateral prefrontal cortex: architectonic and functional organization. Philos Trans R Soc Lond B Biol Sci. 2005; 360:781–795. [PubMed: 15937012]

Petrides, M. Broca's area in the human and the non-human primate brain. In: Grodzinsky, Y.; Amunts, K., editors. Broca's Region. Oxford University Press; New York: 2006. p. 31-46.

Petrides M, Cadoret G, Mackey S. Orofacial somatomotor responses in the macaque monkey homologue of Broca's area. Nature. 2005; 435:1235–1238. [PubMed: 15988526]

Petrides M, Pandya DN. Projections to the frontal cortex from the posterior parietal region in the rhesus monkey. J Comp Neurol. 1984; 228:105–116. [PubMed: 6480903]

Petrides M, Pandya DN. Association fiber pathways to the frontal cortex from the superior temporal region in the rhesus monkey. J Comp Neurol. 1988; 273:52–66. [PubMed: 2463275]

Petrides, M.; Pandya, DN. Comparative architectonic analysis of the human and the macaque frontal cortex. In: Boller, F.; Grafman, J., editors. Handbook of Neuropsychology. Elsevier; Amsterdam: 1994. p. 17.58

Petrides M, Pandya DN. Comparative cytoarchitectonic analysis of the human and the macaque ventrolateral prefrontal cortex and corticocortical connection patterns in the monkey. Eur J Neurosci. 2002; 16:291–310. [PubMed: 12169111]

Petrides M, Pandya DN. Distinct parietal and temporal pathways to the homologues of Broca's area in the monkey. PLoS Biol. 2009; 7:e1000170. [PubMed: 19668354]

Rasmussen, T.; Milner, B. Clinical and surgical studies of the cerebral speech areas in man. In: Zulch, KJ.; Creutzfeldt, O.; Galbraith, GC., editors. Cerebral Localization. Springer-Verlag; Berlin: 1975.

Rizzolatti G, Craighero L. The mirror-neuron system. Annu Rev Neurosci. 2004; 27:169–192. [PubMed: 15217330]

Rizzolatti G, Fadiga L, Gallese V, Fogassi L. Premotor cortex and the recognition of motor actions. Brain Res Cogn Brain Res. 1996; 3:131–141. [PubMed: 8713554]

Roy AK, Shehzad Z, Margulies DS, Kelly AM, Uddin LQ, Gotimer K, Biswal BB, Castellanos FX, Milham MP. Functional connectivity of the human amygdala using resting state fMRI. Neuroimage. 2009; 45:614–626. [PubMed: 19110061]

Saur D, Kreher BW, Schnell S, Kummerer D, Kellmeyer P, Vry MS, Umarova R, Musso M, Glauche V, Abel S, Huber W, Rijntjes M, Hennig J, Weiller C. Ventral and dorsal pathways for language. Proc Natl Acad Sci U S A. 2008; 105:18035–18040. [PubMed: 19004769]

Shehzad Z, Kelly AM, Reiss PT, Gee DG, Gotimer K, Uddin LQ, Lee SH, Margulies DS, Roy AK, Biswal BB, Petkova E, Castellanos FX, Milham MP. The resting brain: unconstrained yet reliable. Cereb Cortex. 2009; 19:2209–2229. [PubMed: 19221144]

Skudlarski P, Jagannathan K, Calhoun VD, Hampson M, Skudlarska BA, Pearlson G. Measuring brain connectivity: diffusion tensor imaging validates resting state temporal correlations. Neuroimage. 2008; 43:554–561. [PubMed: 18771736]

Steinley D. Stability analysis in K-means clustering. Br J Math Stat Psychol. 2008; 61:255–273. [PubMed: 17535479]

Tomaiuolo F, MacDonald JD, Caramanos Z, Posner G, Chiavaras M, Evans AC, Petrides M. Morphology, morphometry and probability mapping of the pars opercularis of the inferior frontal gyrus: an in vivo MRI analysis. Eur J Neurosci. 1999; 11:3033–3046. [PubMed: 10510168]

Uddin LQ, Mooshagian E, Zaidel E, Scheres A, Margulies DS, Kelly AM, Shehzad Z, Adelstein JS, Castellanos FX, Biswal BB, Milham MP. Residual functional connectivity in the split-brain revealed with resting-state functional MRI. Neuroreport. 2008; 19:703–709. [PubMed: 18418243]

van den Heuvel M, Mandl R, Hulshoff Pol H. Normalized cut group clustering of resting-state FMRI data. PLoS One. 2008a; 3:e2001. [PubMed: 18431486]

van den Heuvel M, Mandl R, Luigjes J, Hulshoff Pol H. Microstructural organization of the cingulum tract and the level of default mode functional connectivity. J Neurosci. 2008b; 28:10844–10851. [PubMed: 18945892]

van den Heuvel MP, Mandl RC, Kahn RS, Hulshoff Pol HE. Functionally linked resting-state networks reflect the underlying structural connectivity architecture of the human brain. Hum Brain Mapp. 2009; 30:3127–3141. [PubMed: 19235882]

Vincent JL, Kahn I, Snyder AZ, Raichle ME, Buckner RL. Evidence for a frontoparietal control system revealed by intrinsic functional connectivity. J Neurophysiol. 2008; 100:3328–3342. [PubMed: 18799601]

Vincent JL, Patel GH, Fox MD, Snyder AZ, Baker JT, Van Essen DC, Zempel JM, Snyder LH, Corbetta M, Raichle ME. Intrinsic functional architecture in the anaesthetized monkey brain. Nature. 2007; 447:83–86. [PubMed: 17476267]

Warren JE, Wise RJ, Warren JD. Sounds do-able: auditory-motor transformations and the posterior temporal plane. Trends Neurosci. 2005; 28:636–643. [PubMed: 16216346]

Wernicke, C. Der aphasische Symptomenkomplex. Cohn and Weigert; Breslau: 1874.

Xiang HD, Fonteijn HM, Norris DG, Hagoort P. Topographical Functional Connectivity Pattern in the Perisylvian Language Networks. Cereb Cortex. 2009

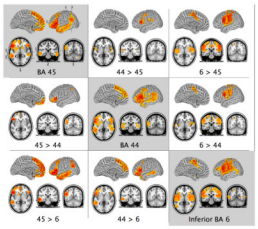

Figure 1.
Patterns of group-level resting state functional connectivity associated with the three manually-selected ventrolateral frontal ROIs, and the results of direct contrasts between them ($Z > 2.3$; cluster significance $p < 0.05$, corrected). Images are in MNI152 space and are shown according to neurological convention (right is right).

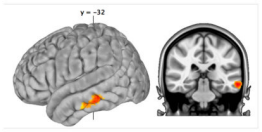

Figure 2.

Results of the direct comparison between BA 45 and 44, after restricting our analysis to the left temporal lobe ($Z > 2.3$; cluster significance $p < 0.05$, corrected for a volume of $22768mm^3$). This small volume-corrected comparison revealed significantly greater RSFC between BA 45 and the middle temporal gyrus, relative to BA 44.

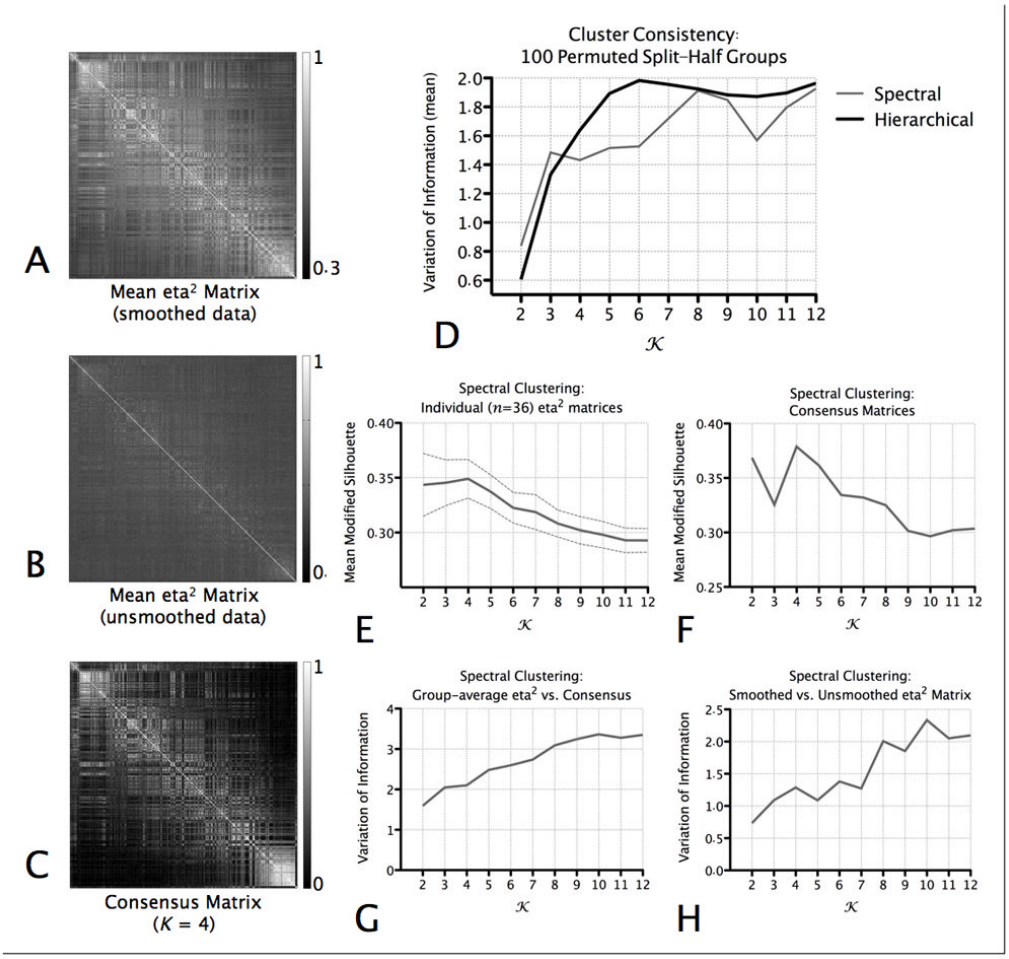

Figure 3.

Clustering Indices. (A) The group-average (mean) of the individual eta^2 matrices computed on the basis of the smoothed resting state data. (B) The group-average of the individual eta^2 matrices computed on the basis of the unsmoothed resting state data. (C) The consensus matrix for *K*=4. This matrix represents, when *K*=4, the stability with which pairs of voxels were assigned to the same cluster across individuals. (D) For each value of *K*, we assessed the similarity of the cluster solutions generated for Group 1 (*n* = 18) and Group 2 (*n* = 18) in the permuted-groups split-half comparison procedure using the Variation of Information (VI) metric (Meila, 2007). The graph plots the mean VI across 100 permuted groups, for each *K*, for the hierarchical and spectral clustering algorithms. Lower VI scores indicate better similarity (consistency) between the solutions computed for each group. (E) Mean (and standard deviation) of the modified silhouette for each value of *K*, for cluster solutions produced when the spectral clustering algorithm was applied *to each individual's* eta^2 matrix. (F) Modified silhouette values computed for clustering solutions computed on the basis of the consensus matrices, for each value of *K*. (G) Similarity between the cluster assignments for the group-average (mean) of the individual eta^2 matrices (i.e., shown in A) and those for the consensus matrices (example shown in C). (H) Similarity between the cluster assignments for the group-average (mean) of the individual eta^2 matrices computed on the basis of the smoothed resting state data (i.e., shown in A) and the those computed on the basis of the unsmoothed resting state data (example shown in B).

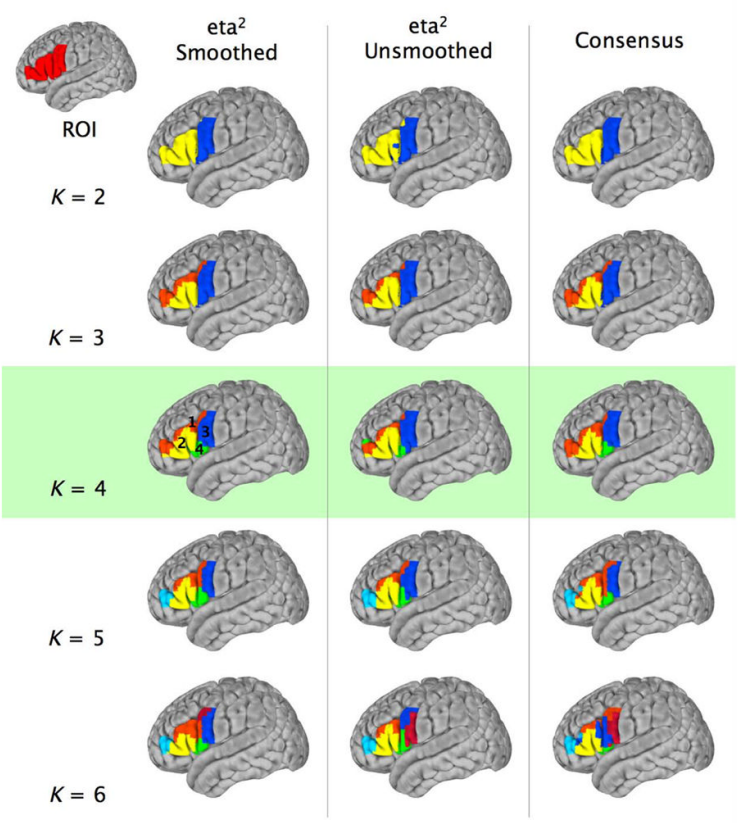

Figure 4.

Surface maps (MNI152 brain) for the spectral clustering solutions for $K = 2{:}6$ for (1) the group-average of individual participants' eta^2 matrices computed on the basis of the smoothed resting state data (eta^2 Smoothed – first column); (2) the group-average of the individual eta^2 matrices computed on the basis of the unsmoothed resting state data (eta^2 Unsmoothed – second column); and (3) the consensus matrix (Consensus – third column).

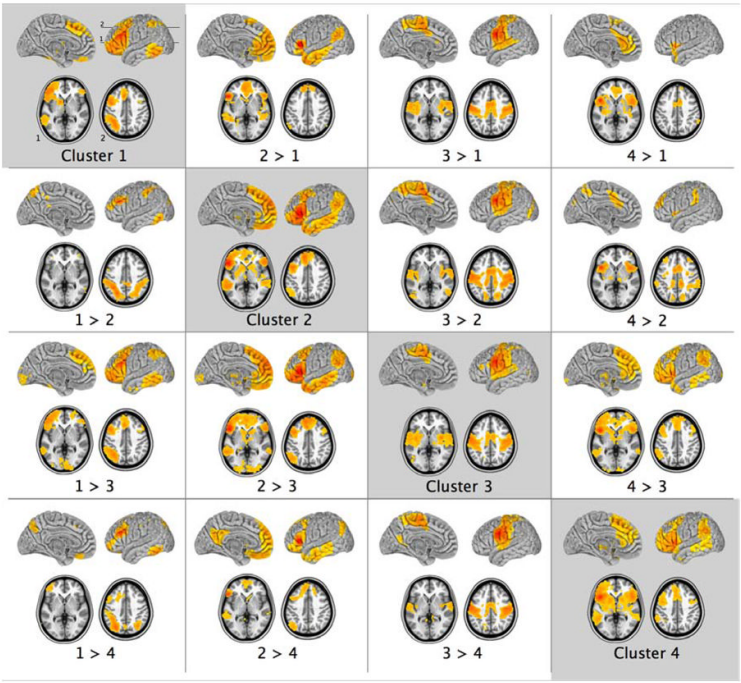

Figure 5.

Patterns of group-level resting state functional connectivity and the results of direct contrasts for the four seed ROIs located at the centers-of-mass of the group-average $K = 4$ spectral clustering solution. The clusters are marked in Figure 4 and correspond to: the superior part of the inferior frontal gyrus (IFG), bordering the inferior frontal sulcus (Cluster 1); the lateral pars opercularis and pars triangularis (Cluster 2); inferior precentral cortex (Cluster 3); and a fourth region extending medially within the Sylvian fissure from the inferior-most tip of ventral premotor cortex and the pars opercularis towards the anterior insula (Cluster 4). $Z > 2.3$; cluster significance $p < 0.05$, corrected. Images are in MNI152 space and are shown according to neurological convention (right is right). The numbers (top left panel) indicate the positions of the axial slices shown in the lower portion of each panel.

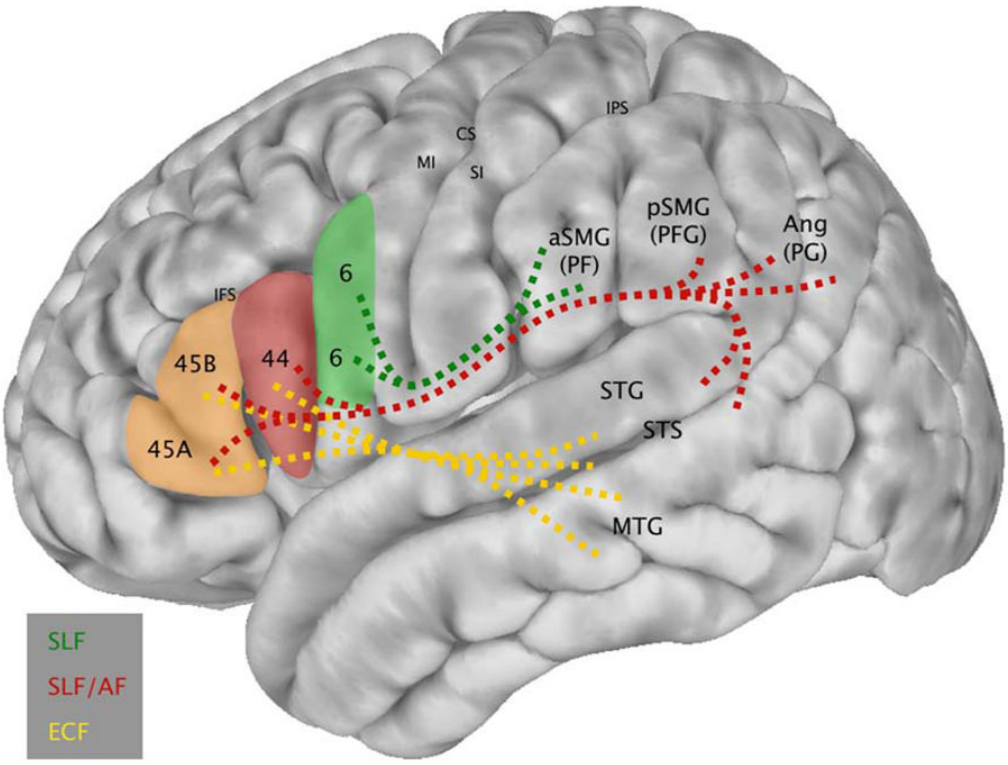

Figure 6.

Schematic diagram integrating the observed patterns of functional connectivity between BAs 6, 44, and 45 and perisylvian parietal and temporal regions (i.e., the results of the present study) with information concerning the white matter tracts that join these regions, derived from experimental anatomical tracer studies in the macaque monkey that can demonstrate the precise origin, trajectory and termination of axonal fiber systems (Petrides & Pandya, 2009). Lines are dashed to indicate that the white matter pathways underlying the observed functional connectivity are hypothesized, but not measured directly in the present study. SLF: Superior Longitudinal Fasciculus; AF: Arcuate Fasciculus; ECF: Extreme Capsule Fasciculus.